2nd International Symposium on Magnetic Beaing
July 12-14, 1990, Tokyo, Japan

DESIGN AND PERFORMANCE OF A HIGH SPEED MILLING SPINDLE IN DIGITALLY CONTROLLED ACTIVE MAGNETIC BEARINGS

R. SIEGWART[1], R. LARSONNEUR[1], A. TRAXLER[2]

[1]Institute of Robotics, Swiss Federal Institute of Technology (ETH), 8092 Zurich, Switzerland
[2]MECOS TRAXLER AG, CH-8400 Winterthur, Switzerland

ABSTRACT

High Speed Cutting (HSC) finds increasing industrial interest due to its capability of drastically reducing production times. HSC uses up to ten times higher cutting speeds and allows greatly improved metal removal capacity. Furthermore, cutting forces are lower and surface quality is better than in the conventional cutting process. Active magnetic bearings (AMB) allow much higher surface speeds than conventional ball bearings and are therefore perfectly suitable for HSC applications. After a short introduction into HSC this paper describes the overall design of a magnetically suspended milling spindle with a power of 35 kW at 40'000 rpm and a cutting force of 1000 N. Mechanical spindle design and related problems such as material strength and rotor stiffness are investigated. "Conditioning" of the AMB rotor system in terms of *observability* and *controllability* is discussed. Linear and nonlinear characteristics of the *electro-magnetic actuator* (bearing magnet and power amplifier as one unit) are described. Digital controller layout is based on a layout method (*SPOC-D*) for *structurally predefined* discrete-time control systems. This method optimizes feedback parameters of arbitrary *low order* control schemes for *high order* plants. Results of milling tests are presented, showing the advantages of AMBs in HSC technology.

1. INTRODUCTION

Experiments performed at different research centers since the late seventies showed that the cutting process of materials such as aluminum and plastic can be substantially improved by increasing the cutting speed [1,2]. Based on these results, a new cutting technology, the *High Speed Cutting* (HSC), was developed and introduced into industrial applications during the past decade.

The main advantages of High Speed Cutting are:

- higher relative cutting volume
- lower cutting time
- lower cutting forces
- reduced loading of cutting tool and cutting machine
- reduced tendency for chattering
- less warming of the work piece as the removed chip carries more heat
- lower production cost

Despite of the high standard already reached in HSC technology, considerable research is still going on, particularly aimed at increasing cutting speeds and at optimizing the whole cutting process. Therefore, a clear trend towards milling spindles reaching higher rotational speeds, needing less maintenance and showing additional features such as *"in-process-control"* is discernible [3,4,5].

Active magnetic bearings (AMB) seem to be a very suitable tool for the challenging application of HSC. However, high demands are placed on actuator, controller and rotor design. The great potential of AMB technology in this field has been shown by the first analog-control AMB milling spindle developed by *S2M* in cooperation with the *Technical University of Darmstadt* [6].

2. MILLING SPINDLE DESIGN

2.1 HSC Milling Spindle Requirements

For almost all technically interesting HSC operations, tools with diameters between 10 and 60 mm and ISO 40 tool holders are used. To date, conventional ball bearing milling spindles with ISO 40 tool-holders can reach rotational speeds ranging from 15'000 to 20'000 rpm at a maximum cutting power up to 30 kW. However, *optimal* cutting speed can most often not be reached using conventional milling spindles due to the limited surface speed of the ball bearings. This is especially the case for small tool diameters. By using the latest *ceramic bearing* technology, a 20 to 30% increase in maximum rotational speed is possible, but life time of such bearings is limited to a few thousands of hours at best.

For a further important step towards higher rotational speeds using ISO 40 tool holders, electro-magnetic bearings seem to be the only feasible solution. Apart from the higher rotational speed, AMBs feature long lifetime due to the complete lack of mechanical wear. In addition, by using the force and displacement signals available in an AMB system, new insights into the whole cutting process can be obtained.

2.2 Overall Design Concept

The AMB milling spindle (figure 1) described in this paper was developed at the *Swiss Federal Institute of Technology (ETH)* and built in cooperation with the milling spindle manufacturer *IBAG Zürich AG* specialized in HSC technology [7]. The spindle design features the following characteristics:

- maximum rotational speed: 40'000 rpm
- maximum cutting power: 35 kW
- maximum cutting force: 1000 N
- integrated ISO 40 tool change system
- digital control using a DSP

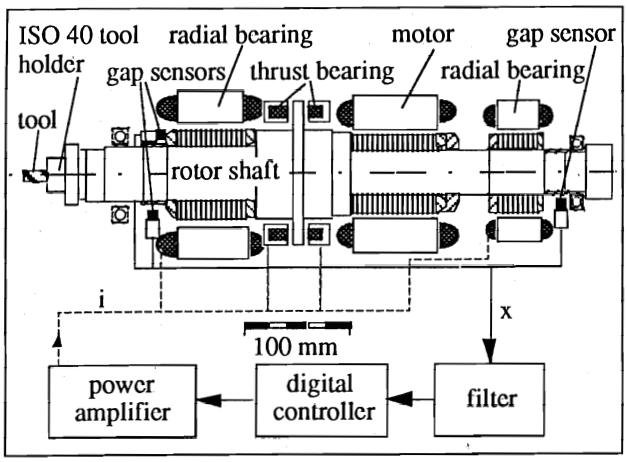

Figure 1: AMB milling spindle system

In order to find an optimal solution for the demanding task of developing an AMB high speed milling spindle, special emphasis was put on mechanical rotor design (high static and dynamic stiffness of the rotor shaft), on AMB actuators (bearing and power amplifier) and on digital control.

2.3 Mechanical Rotor Design

In order to cope with the static and dynamic cutting forces on the one hand and to reduce vibration effects on the other hand, the spindle rotor must be made as stiff as possible. The consequence of this basic design rule is a *short rotor* with a shaft diameter as *large* as possible. Therefore, due to centrifugal forces, the rotor elements are stressed up to their mechanical limits given by the material strength.

In order to reduce eddy current and hysteresis loss, motor and magnetic bearing elements consist of soft magnetic iron sheets which have to be *shrink-fitted* on to the rotor core. These lamination sheets do not increase rotor stiffness; they only add mass to the rotor core and, therefore, lead to decreased natural frequencies of the bending modes. Hence, from the stiffness point of view, the inner diameter of motor and bearing lamination sheets must be made as large as possible.

From the material exploitation point of view, however, thicker lamination sheets would allow higher surface speeds, since reference stress at the inner edge of the lamination sheets increases with the inner sheet diameter [8].

Figure 2 shows the speed dependency of radial and reference stress at the inner edge of the lamination sheets (front bearing). The material strength of the soft magnetic iron ranges near 400 N/mm^2.

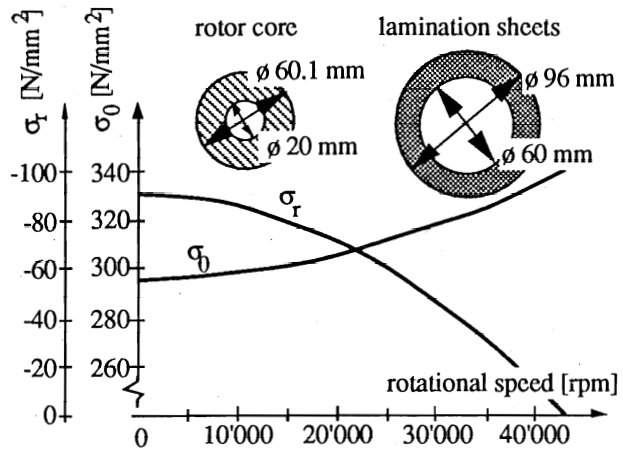

Figure 2: Radial stress σ_r at the contact between rotor core and lamination sheets and maximum reference stress σ_0 at the inner edge of the lamination sheets for the front radial bearing

The mechanical design of the AMB spindle rotor (figures 1 and 3) was dominated be the following constraints:

- highest possible yield strength for motor and bearing lamination sheets
- highest possible motor power and bearing forces
- ISO 40 tool system
- maximum rotational speed below first bending mode
- easy assembly of the whole spindle unit

The eigenfrequencies and corresponding mode shapes of the relevant first two bending modes are plotted in figure 3.

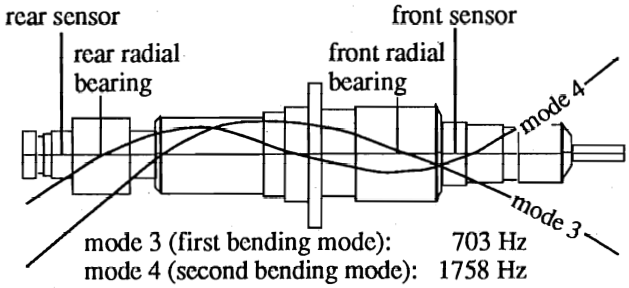

Figure 3: Eigenfrequencies and corresponding mode shapes of the AMB milling spindle

As it can be concluded from figure 3, the first elastic bending mode is very close to the maximum rotational speed (666 Hz) and must therefore be considered the most critical element of the rotor design. This also shows that further investigations must be made for future

applications, especially in the field of high speed motor elements featuring both high power and high mechanical stiffness.

2.4 Conditioning of an AMB Rotor in Terms of Observability and Controllability

Active magnetic bearings can be considered elements suitable for *supplying* energy *to* or for *removing* energy *from* the supported rotor. The "energy space" of the rotor can be subdivided into its different modes of motion, and the performance of energy transfer to or from these modes is represented by the so-called *controllability* and *observability* properties.

Generally, a non-turning rotor in AMBs can be described by the following set of linear differential equations in modal space (vector $\mathbf{x}$ of order n):

$$\ddot{\mathbf{x}} + \mathrm{diag}(2\delta_i)\,\dot{\mathbf{x}} + \mathrm{diag}(\omega_i^2)\,\mathbf{x} = \tilde{\mathbf{B}}\,\mathbf{u}\,; \quad i = 1 \ldots n$$
$$\mathbf{y} = \tilde{\mathbf{C}}\,\mathbf{x} \qquad (1)$$

$\tilde{\mathbf{B}}$: control matrix
$\tilde{\mathbf{C}}$: measurement matrix
δ_i: modal damping coefficients
ω_i: eigenfrequencies

We assume that the rotor is suspended with a very low stiffness ($\omega_{1,2} << \omega_3 \ldots \omega_n$) and that all eigenmodes show low damping δ_i, so that the open-loop system is stable. These assumptions have no relevant effect on controllability and observability but facilitate discussion of the system properties.

For the rotor system described by (1) the following state space description can be derived:

$$\dot{\mathbf{z}} = \mathbf{A}\,\mathbf{z} + \mathbf{B}\mathbf{u}$$
$$\mathbf{y} = \mathbf{C}\cdot\mathbf{z} \qquad (2)$$

$$\mathbf{z} = \begin{bmatrix} \mathbf{x} \\ \mathrm{diag}(1/\omega_i)\dot{\mathbf{x}} \end{bmatrix}$$

$$\mathbf{A} = \begin{bmatrix} \varnothing & \mathrm{diag}(\omega_i) \\ -\mathrm{diag}(\omega_i) & -\mathrm{diag}(2\,\delta_i) \end{bmatrix}$$

$$\mathbf{B} = \begin{bmatrix} \varnothing \\ \mathrm{diag}(\frac{1}{\omega_i})\,\tilde{\mathbf{B}} \end{bmatrix}\ ; \quad \mathbf{C} = \begin{bmatrix} \tilde{\mathbf{C}} & \varnothing \end{bmatrix}$$

The symbols used in (2) are:

- **z**: state vector of modes and scaled velocity (order 2n)
- **y**: measured displacement
- **A**: system matrix of weakly supported rotor
- **B**: influence matrix of bearing forces
- **C**: measurement matrix

For a system described by (2) with **A** being a stable matrix one can define the *observability gramian* $\mathbf{W}_o$ and the *controllability gramian* $\mathbf{W}_c$ [9,10] as follows:

$$\mathbf{W}_o = \int_0^\infty e^{\mathbf{A}^T t}\,\mathbf{C}^T\,\mathbf{C}\,e^{\mathbf{A}t}\,dt = \mathbf{U}\,\Sigma_o^2\,\mathbf{U}^T$$

$$\mathbf{W}_c = \int_0^\infty e^{\mathbf{A}t}\,\mathbf{B}\,\mathbf{B}^T\,e^{\mathbf{A}^T t}\,dt = \mathbf{V}\,\Sigma_c^2\,\mathbf{V}^T$$

$$\mathbf{U} = [\mathbf{u}_1 \ldots\ldots \mathbf{u}_{2n}]\,;\ \mathbf{U}^T\mathbf{U} = \mathbf{I}\,;\ \Sigma_o^2 = \mathrm{diag}(\sigma_{oi}^2)\,;\ i = 1\ldots 2n$$
$$\mathbf{V} = [\mathbf{v}_1 \ldots\ldots \mathbf{v}_{2n}]\,;\ \mathbf{V}^T\mathbf{V} = \mathbf{I}\,;\ \Sigma_c^2 = \mathrm{diag}(\sigma_{ci}^2)\,;\ i = 1\ldots 2n \qquad (3)$$

The quadratic form η_o

$$\eta_o = \mathbf{z}_0^T\mathbf{W}_o\mathbf{z}_0 \qquad (4a)$$

represents the total signal "energy" (L^2 norm) seen at the system output due to the initial state $\mathbf{z}_0$, whereas η_c

$$\eta_c = \mathbf{z}^T\mathbf{W}_c^{-1}\mathbf{z} \qquad (4b)$$

denotes the minimum control energy required to reach the state **z** [17]. Expressions (4a) and (4b) are quantitative measures for observability and controllability of the state vector **z**. Eigenvectors $\mathbf{u}_i$ and $\mathbf{v}_i$ in (3) denote observable and controllable directions with associated energy σ_{oi}^2 for the observability gramian and σ_{ci}^2 for the controllability gramian.

The so-called *condition numbers* κ_o and κ_c given by

$$\kappa_o = \frac{\sigma_{o\max}^2}{\sigma_{o\min}^2}\ ; \quad \kappa_c = \frac{\sigma_{c\max}^2}{\sigma_{c\min}^2} \qquad (5)$$

are quantitative numbers to determine the observability and controllability properties of the rotor system. High condition numbers correspond to a poor conditioning.

For a rotor system in modal state space description (2) the eigenvectors of the observability and controllability gramians $\mathbf{u}_i$ and $\mathbf{v}_i$ are equal to the i-th (normalized) eigenvector of the system matrix **A**. Therefore the singular values σ_{oi}^2 and σ_{ci}^2 are equal to the signal energy η_o and the control energy η_c respectively for an assumed unit initial state in direction of the i-th eigenmode. Moreover, for small modal damping coefficients δ_i, the singular values are directly proportional to the inverse of the damping δ_i.

Figures 4 and 5 show the singular values σ_{oi}^2 and σ_{ci}^2 of the observability and controllability gramians related to the eigenmodes of the milling spindle rotor (modes 1 and 2 are the rigid body modes). The singular values for front and rear bearings are plotted individually to show the influence of each single magnetic bearing on the total observability and controllability status. For example, mode 4 is very

poorly observable but quite well controllable from the front bearing, a fact which is also reflected by the mode shapes of the milling spindle rotor (figure 3).

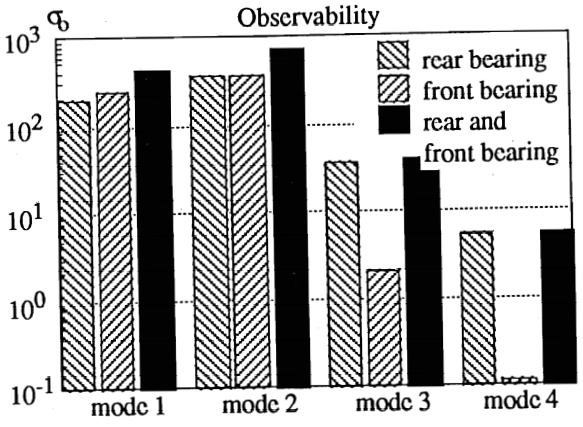

Figure 4: Observability of the AMB milling spindle rotor

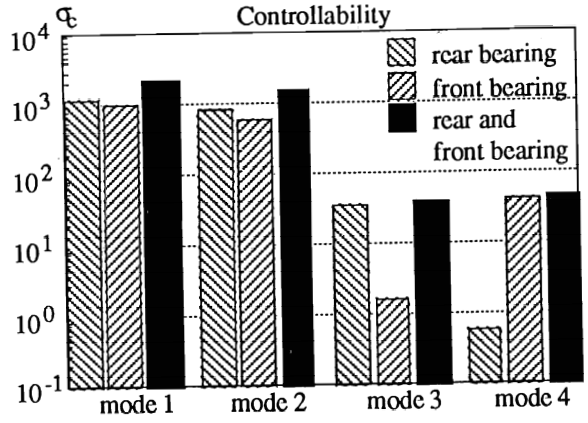

Figure 5: Controllability of the AMB milling spindle rotor

The gramians are also a useful tool for model reduction [16]: (stable) eigenmodes with very poor observability *and* controllability can be neglected.

For both observability and controllability one can find the corresponding condition numbers for the milling spindle rotor applying expression (5):

$\kappa_o = 150$
$\kappa_c = 70$

Observability of the milling spindle rotor is poorer than controllability. This is particularly caused by the 2nd elastic eigenmode (4th mode) which shows a *vibration node* near the front sensor location. It is therefore useful to *cut off* the sensor signal between the third and forth mode by means of an appropriate low pass filter.

Although controllability of the milling spindle rotor is rather good, the effectiveness of tuning for the higher modes will be decreased by the limited bandwidth of the AMB actuator. This is investigated in the next section.

3. AMB Actuator Layout

3.1 Dynamic Bearing Force

The force-current-displacement relationship of the magnetic bearing force F produced by a pair of opposing electro-magnetic coils using current control (figure 6) is given by the following well known expression:

$$F = k\left[\left(\frac{i_0+i_x}{s-x}\right)^2 - \left(\frac{i_0-i_x}{s+x}\right)^2\right] \tag{6}$$

The constant k depends on the bearing design parameters, i_0 is the the nominal current (pre-magnetization), i_x is the control current, s is the nominal air gap and x is the rotor displacement from the unstable nominal equilibrium position.

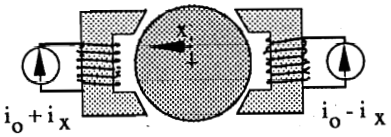

Figure 6: AMB current control

Since coil resistance can be neglected, one can obtain for the related coil voltages u^+ and u^-:

$$u^+ = k_\Delta k \frac{\partial}{\partial t}\left(\frac{i_0+i_x}{s-x}\right);\quad u^- = k_\Delta k \frac{\partial}{\partial t}\left(\frac{i_0-i_x}{s+x}\right) \tag{7}$$

The constant $k_\Delta \approx 1$ is a correction term which takes into consideration the permeability of the iron and possible geometric properties [11].

In order to describe the bearing force dynamics, the time-derivative of the bearing force given by (6) can be formulated using expression (7):

$$\frac{\partial F}{\partial t} = \frac{2}{k_\Delta}\left[\left(\frac{i_0+i_x}{s-x}\right)u^+ - \left(\frac{i_0-i_x}{s+x}\right)u^-\right] \tag{8}$$

Hence, the maximum dynamic bearing force near the nominal rotor position (x = 0) can be derived from (8):

$$\frac{\partial F}{\partial t} \approx 2\,\frac{i_0\, u_{max}}{s} \tag{9}$$

$$u^+ = u_{max}\,;\; u^- = -u_{min}\,;\; k_\Delta \approx 1$$

With a nominal current i_0 being equal to the half maximum current i_{max}, the following relation between power P of the power amplifier and bearing force dynamics is obtained:

$$\frac{\partial F}{\partial t} = \frac{i_{max}\, u_{max}}{s} = \frac{P}{s} \tag{10}$$

Assuming the dynamic bearing force to be sinusoidal with frequency f and amplitude F_0, equation (10) can also be written as:

$$F_{0max} = \frac{1}{2\pi f}\frac{P}{s} \tag{11}$$

Expressions (10) and (11) are rather simple and helpful relations for the design of an AMB actuator. This is shown along with the milling spindle example in the following section.

3.2 Actuator Layout for the Milling Spindle

As mentioned in section 2.2 a maximum static cutting force of 1000 N must be realizable with the AMB milling spindle. In addition, bearing forces must cover a wide dynamic range in order to achieve the required stiffness and damping up to the first elastic bending mode.

The related maximum bearing forces are around 1000 N for the rear bearing and 2000 N for the front bearing. Assuming an AMB actuator bandwidth up to 1 kHz (first bending mode is located at 703 Hz), i.e. providing the maximum bearing force over this whole frequency range, the required amplifier power can be calculated by application of expression (11):

$P_{max} = 2.4$ kVA (rear bearing)
$P_{max} = 4.8$ kVA (front bearing)

These required amplifier powers are quite large, and to date, such amplifiers are not available on the market. Therefore, new switched type power amplifiers with a maximum current of 8 A, a voltage of 310 V and a switching rate of 100 kHz were developed. Thus, a power of 2.5 kVA per bearing channel is achieved, only matching the requirements of the rear bearing. However, since controllability of the first elastic bending mode is much better for the rear than for the front magnetic bearing (figure 5), sufficient damping should be provided using the mentioned power amplifier and an appropriate control algorithm (section 4).

3.3 Nonlinear Model of the AMB Actuator

Power amplifiers are rather often the most limiting component in an AMB system. Because of their low loss, switched amplifiers using current control are most commonly used for AMB systems, especially in the case of high power applications. Besides current control, other possibilities such as voltage or flux control are possible which, for some applications, can improve AMB performance [12,13,14].

Figure 7 shows a schematic diagram of the AMB actuator including bearing coil and nonlinear amplifier logic.

Coil voltage u is determined by the (generally small) coil resistance R_{cu}, the current i and the switched amplifier voltage u_{out}:

$$u = u_{out} - R_{cu}\, i \tag{12}$$

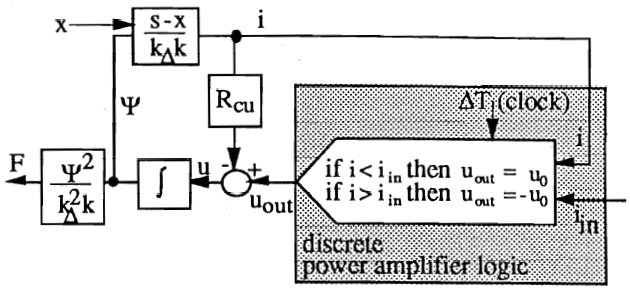

Figure 7: Schematic diagram of the AMB actuator including one bearing coil and switched power amplifier with current control

By integrating the coil voltage over time one obtains the flux linkages Ψ:

$$\Psi = N\,\Phi = \int u\, dt \tag{13}$$

Coil inductivity L can be derived from (13) using the definition $\Psi = L\, i$ (see also figure 7):

$$i = \frac{\Psi}{L} = \frac{(s-x)}{k_\Delta k}\,\Psi \tag{14}$$

$$L = \frac{k_\Delta k}{(s-x)} \tag{15}$$

By introducing Ψ in expression (6) for only one bearing coil, the AMB force can be expressed by the flux linkage and the AMB constants k and k_Δ:

$$F = \frac{1}{k_\Delta^2 k}\,\Psi^2 \tag{16}$$

Simulations with this nonlinear AMB actuator model for the milling spindle are shown in section 5 and compared with a standard linear model. The behavior of the electromagnetic coil is simulated as a continuous-time system, whereas the logic of the switched power amplifier must be considered as a discrete-time system (figure 7).

4. Discrete-Time Controller Layout

A typical property of AMB systems is that only very few system states, most often two displacement signals in each movement plane, are measurable. Thus, especially in the case of flexible rotor structures, the plant order is much higher than the number of output signals available.

A well-known control theoretical consequence resulting from too few output signals being available on the one hand, and from the necessity of achieving enough damping up to high frequencies on the other hand, is that an observer-based state feedback should be implemented in order to include the full system dynamics. However, in case of digital control, such *high order* controller structures will

require a high number of necessary computations, so that only *low sampling rates* can be achieved. Consequently, simpler *low order* discrete-time dynamic output schemes must be provided, which, despite of their low order, take into account the *full dynamics* of the high order plant.

Many layout techniques for discrete-time low order controllers presently available are based on *quasi-continuous approximations* of well-known continuous-time low order control schemes. This approach rather often results in unsatisfactory dynamic behavior of the closed-loop system and, in some cases, may even lead to *instability*.

For the AMB milling spindle the so-called SPOC-D controller layout method was applied (**S**tructure-**P**redefined **O**ptimal **C**ontrol for **D**iscrete Systems). This method was first presented in [15]; its detailed description can be found in [8]. The basic properties of the layout method can be summarized as follows:

Order and structure of the discrete-time controller for the nominal high order plant model are predefined *prior* to the controller layout. This predefinition can be made *freely* according to *practical needs*. In the subsequent controller layout, a parameter optimization is performed taking into account the dynamics of the high order plant as well as those of the low order controller.

In addition, the SPOC-D method allows to include control parameter interdependencies *directly* into the optimization process in order to achieve system properties such as

- specific static magnetic bearing stiffness
- specific frequency domain behavior of a decentralized feedback path (gain and phase at a given frequency, noise rejection at high frequencies for robustness, etc.)

Figure 8 illustrates the decentralized controller performance achieved using SPOC-D. The optimized controller transfer function (curve 2) is compared with a discrete-time PD approximation (curve 1). The traditional PD approximated controller shows high gain at high frequencies and, therefore, generates noise. For the SPOC-D optimized controller, the conditions of low noise at high frequencies as well as of the static bearing stiffness were included as additional control parameter interdependencies in the optimization process. Furthermore, the optimized controller features better phase lead in the frequency mid-range. Both, low noise and better phase lead provide an additional amount of robustness for the AMB milling spindle.

The eigenvalues of the closed-loop system with SPOC-D optimized controller are:

- $\lambda_1 =$ -48 ± 133 Hz (rigid body mode)
- $\lambda_2 =$ -174 ± 333 Hz (rigid body mode)
- $\lambda_3 =$ -151 ± 812 Hz (1st bending mode)
- $\lambda_4 =$ -5 ± 1753 Hz (2nd bending mode)

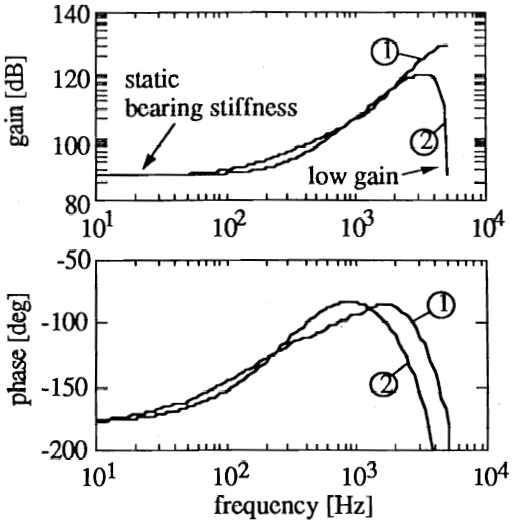

Figure 8: Bode plots of third order decentralized PD controller (1) and of SPOC-D optimized controller (2) with same order

Damping of the two rigid body modes and of the first bending mode are satisfactory, whereas the damping of the second bending mode turns out to be rather small. This is caused by the limited controller and actuator bandwidths and by the poor controllability and observability of the 2nd bending mode using decentralized feedback. However, additional damping of this mode, not included in the model description, is provided by the material's internal damping.

5. RESULTS

Owing to a rotor design which reaches the material strength limits, to the switched power amplifier, to the high sampling rate achieved with a DSP and to the SPOC-D optimized decentralized controller, a HSC milling spindle in AMBs was realized [7]. Compared with conventional ball bearing HSC milling spindles with same cutting power, the rotational speed was doubled, so that lower cutting forces, a higher metal removal rate and optimal surfaces on the work piece could be reached.

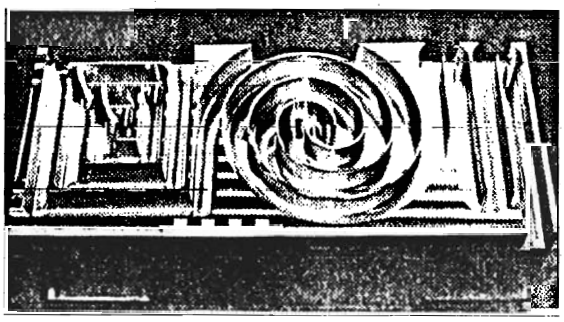

Figure 9: Integral aluminum work piece with straps of 2 mm thickness and of 27 mm height

Figure 9 shows a typical HSC work piece, cut with a miller of 20 mm diameter at cutting speed of 2300 m/min. The whole cutting process took 72 seconds. A cutting speed of over 6000 m/min and a removal rate of more than 1600 cm^3/min were reached applying different tools.

In figure 10 the dynamic compliance of the AMB milling spindle is compared with a conventional milling spindle featuring the same *related cutting force* K_v. The related cutting force K_v is a comparative value for an average cutting force and can be defined as follows:

$$K_v = \frac{\text{cutting power}}{\text{rotational speed} \cdot \text{tool holder diameter}} \qquad (17)$$

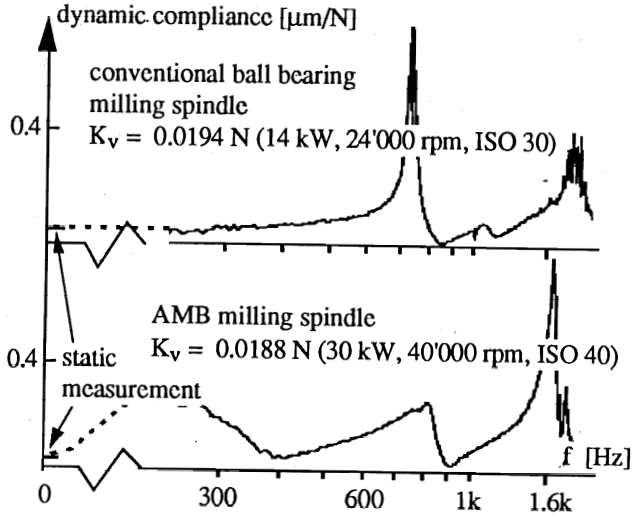

Figure 10: Measured spindle compliance at the tool for a conventional and for the AMB milling spindle

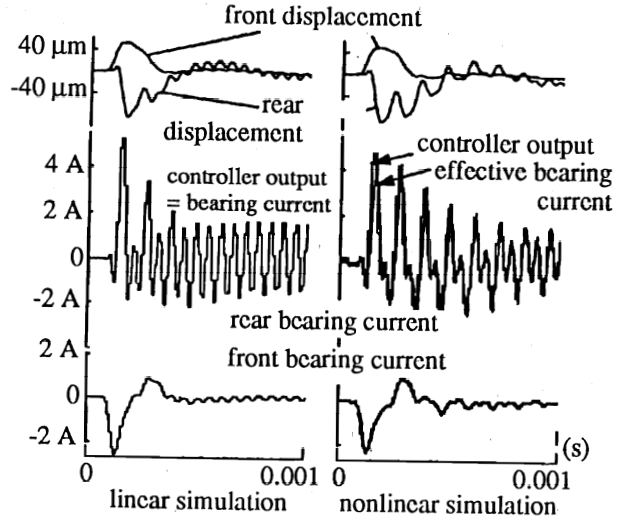

Figure 11: Linear and nonlinear simulations of the system behavior to a force impact at AMB spindle tool

In the low frequency range (50 - 300 Hz) the AMB spindle shows a higher compliance, i.e. a lower dynamic stiffness, than the conventional one. However, this does not affect the cutting process since cutting forces mainly contain higher frequency components. Figure 10 also demonstrates that damping of the first bending mode is much higher for the AMB spindle than for the conventional one, thus, excitations even in the frequency range of the 1st bending mode can be tolerated. Although both AMB and conventional milling spindle have the same related cutting force K_v, the AMB spindle features a cutting power and a rotational speed which are about *twice as high* as for the conventional milling spindle.

Simulations of the AMB system response to a force impact at the spindle tool are shown in figure 11. Power amplifier nonlinearities described in section 3.3 are *included*. Correspondence with measured signals (figure 12) is very good, which points out the precise model worked out for the AMB spindle, especially taking into account the nonlinear amplifier dynamics. Damping reduction of the nonlinear model compared with the linear counterpart is caused by the limited dynamic range of the power amplifier (dynamic current saturation).

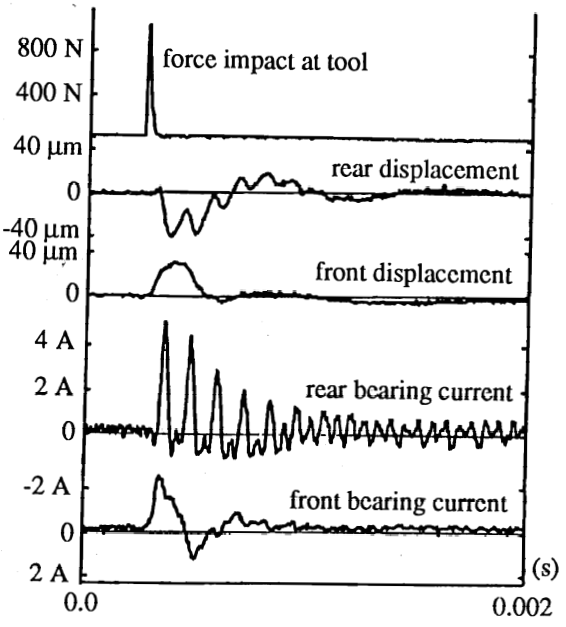

Figure 12: Measured system response to a force impact at AMB spindle tool

6. CONCLUSION

The AMB milling spindle prototype described in this paper has proven the feasibility of contactless support for HSC milling spindles by means of digitally controlled electromagnetic bearings.

The yielded results could be achieved thanks to the introduction of a digital signal processor (DSP) and thanks to a new discrete-time controller layout method in conjunction with a realistic model of the whole system. Furthermore, a specifically developed switched power amplifier and a sophisticated stiff rotor construction have contributed to the good overall performance of the AMB milling spindle system.

Nevertheless, future investigations must be made in the fields of motor elements for high rotational speed and of low cost solutions for power amplifier and digital control systems. New "in-process-control" features based on digital control systems have to be implemented in order to optimize the whole cutting process and thus to create highly automated and reliable systems.

REFERENCES

[1] STEINMETZ E. (Editor): Hochgeschwindigkeitsfräsen von metallischen und nichtmetallischen Werkstoffen, Technische Mitteilungen, vol. 17, 1983

[2] TLUSTY J.: Dynamics of High-Speed Milling, Journal of Engineering for Industry, vol. 108, 1986

[3] GALLIST R.: Hochgeschwindigkeitszerspanung - Entwicklung bis zum Jahr 2000, Technica, 2/1988

[4] SCHULZ H.: Die Vorteile des Hochgeschwindigkeitsfräsens, Technica, 26/1988

[5] VANN C. and M. CUTKOSKY: Closing the Loop in CAD/CAM Integration, proceedings of the USA-Japan Symposium on Flexible Automation, Minneapolis, Minnesota, July 1988

[6] ARNOLD W.: Beitrag zu Entwicklung und Einsatz aktiv magnetgelagerter Hochgeschwindigkeits-Frässpindeln, Thesis TH Darmstadt, 1985

[7] SIEGWART R.: Aktive magnetische Lagerung einer Hochleistungs-Frässpindel mit digitaler Regelung, Thesis ETH No. 8962, Zurich, 1989

[8] LARSONNEUR R.: Design and Control of Active Magnetic Bearing Systems for High Speed Rotation, Thesis ETH No. 9140, Zurich, 1990

[9] BOYD S.: Multivariable System Theory, lecture notes EE364, Stanford, 1990

[10] MOORE B.C.: Principal component analysis in linear systems: Controllability, observability and model reduction, IEEE Transactions on Automatic Control, 2/1981

[11] SIEGWART R. and A. TRAXLER: Möglichkeiten und Grenzen schneller Aktuatoren am Beispiel einer magnetisch gelagerten Hochgeschwindigkeits-Frässpindel, VDI-Berichte Nr. 787, 1989

[12] VISCHER D.: Sensorlose und spannungsgesteuerte Magnetlager, Thesis ETH No. 8665, Zurich, 1988

[13] VISCHER D. and H. BLEULER: A New Approach to Sensorless and Voltage Controlled AMBs Based on Network Theory Concepts, paper submitted to the 2nd International Symposium on Magnetic Bearings, Tokyo, July 1990

[14] ZLATNIK D. and A. TRAXLER: Cost-Effective Implementation of Active Magnetic Bearings, paper submitted to the 2nd International Symposium on Magnetic Bearings, Tokyo, July 1990

[15] LARSONNEUR R. and R. HERZOG: Optimal Design of Structure Predefined Discrete Control for Rotors in Magnetic Bearings (SPOC-D), 1st International Symposium on Magnetic Bearings, Zurich, June 1988

[16] WILLIAMS T.: Closed-Form Grammians and Model Reduction for Flexible Space Structures, IEEE Transactions on Automatic Control, 3/1990

[17] GLOVER K.: All optimal Hankel norm approximations of linear multivariable systems and their L^{∞}-error bounds, Int. J. Control, vol. 39, 6/1984